Neutral-current neutrino-nucleus cross sections based on relativistic nuclear energy density functional

Đapo, Haris; Paar, Nils

Neutral-current neutrino-nucleus cross sections based on relativistic nuclear energy density functional

H. Đapo[1,2,*] and N. Paar[1,†]

[1]*Physics Department, Faculty of Science, University of Zagreb, Croatia*
[2]*Department of Physics, Akdeniz University, TR-07058, Antalya, Turkey*

Background: Inelastic neutrino-nucleus scattering through the weak neutral-current plays an important role in a stellar environment where the transport of neutrinos determines the rate of cooling. Since there are no direct experimental data on neutral-current neutrino-nucleus cross sections available, only the modeling of these reactions provides the relevant input for supernova simulations.

Purpose: To establish a fully self-consistent framework for neutral-current neutrino-nucleus reactions based on a relativistic nuclear energy density functional.

Methods: Neutrino-nucleus cross sections are calculated using a weak Hamiltonian and nuclear properties of initial and excited states are obtained with a relativistic Hartree-Bogoliubov model and a relativistic quasiparticle random phase approximation that is extended to include pion contributions for unnatural parity transitions.

Results: Inelastic neutral-current neutrino-nucleus cross sections for ^{12}C, ^{16}O, ^{56}Fe, ^{56}Ni, and even isotopes $^{92-100}$Mo as well as respective cross sections averaged over distribution of supernova neutrinos.

Conclusions: The present study provides insight into neutrino-nucleus scattering cross sections in the neutral channel, their theoretical uncertainty in view of recently developed microscopic models, and paves the way for systematic self-consistent large-scale calculations involving open-shell target nuclei.

I. INTRODUCTION

Nuclear weak interaction processes play an important role in the evolution of supernova collapse, e.g., electron capture, β decay, and neutrino-nucleus reactions [1]. Neutrino-nucleus scattering through the weak neutral current could provide contributions of relevance in a stellar environment where the transport of neutrinos determines the rate of cooling [1–3]. Recently, inelastic neutrino-nucleus scattering has been introduced in supernova simulations as a novel mode of energy exchange between neutrinos and matter [4–6]. Although this process has no large effect on collapse trajectories, it has a significant contribution to increasing the neutrino opacities, and it strongly reduces the high-energy tail of the neutrino spectrum emitted in the neutrino burst at shock breakout [5]. To date, only a single microscopic framework for the neutral-current neutrino-nucleus scattering, based on the hybrid model [7], has been included in supernova simulations [1]. Since the calculations of weak interaction processes in various theoretical models can result in differences in the reaction rates and cross sections, sometimes larger than an order of magnitude [8–11], providing insight into the neutral-current neutrino-nucleus cross sections from independent models is paramount for assessing the impact of the uncertainties in nuclear structure models on the outcomes of supernova simulations.

Modeling neutrino-induced reactions is also important in view of studies on modern detectors based on neutrino scattering on hadrons and nuclei. The ongoing and planned neutrino detector facilities involve a variety of target materials, induced reactions, and scientific objectives. These include MOON [12], MiniBooNE [13], NEMO [14], MINOS [15], SNO + [16], OPERA [17], LVD (large volume detector) [18], the ORLaND experiment at the Spallation Neutron Source (SNS) [19], NOvA neutrino experiment [20], etc. In addition to charged-current neutrino-induced processes in detectors, another possible reaction channel includes neutral-current neutrino scattering on hadrons and nuclei, resulting, e.g., in small showers of secondary γ radiation and the creation of electron-positron pairs. Although the cross sections in the neutral channel are smaller than in the case of charge-exchange reactions, the understanding of complete detector response necessitates consistent microscopic insight into all relevant processes involved.

Over the past years, several theoretical frameworks have been developed to provide a description of the inelastic neutrino-nucleus scattering in the neutral channel. Due to considerable progress in the shell model Hamiltonians, a number of neutrino-induced reactions have been described, also including various decay channels [21–26]. Random phase approximation (RPA) based on Landau-Migdal force has been employed in calculations of neutrino-induced reaction rates for r-process nuclei, including those in the neutral channel [27,28]. The hybrid model combines the shell model for allowed transitions, with the RPA to account for the forbidden transitions, allowing systematic calculations for a large number of target nuclei [7,25,29,30]. The Hartree-Fock + RPA based fully on the Skyrme functional has been employed in studies of the cross sections for ^{12}C, ^{16}O, and ^{208}Pb [31,32]. In view of developing neutrino detectors and the astrophysical role of neutrino-nucleus reactions, the relevant nuclear matrix elements have recently been revisited in

*haris@akdeniz.edu.tr
†npaar@phy.hr; http://www.phy.pmf.unizg.hr/~npaar

Ref. [33], and employed in studies involving target nuclei ^{40}Ar, ^{56}Fe, $^{92-100}$Mo, and ^{128,130}Te, based on quasiparticle RPA (QRPA) [34–37]. In another recently developed framework based on the Hartree-Fock-Bogoliubov (HFB) model and QRPA, the Brueckner G matrix is employed for a two-body interaction by solving the Bethe-Salpeter equation based on the Bonn CD potential, and pairing correlations have also been taken into account [38–40]. Supernova neutrino-^{56}Fe cross sections in the neutral channel have also been explored in the local density approximation taking into account the Pauli blocking and Fermi motion effects [41]. Relativistic theoretical approaches have been employed in modeling neutral-current neutrino-nucleus cross sections, including the quasielastic regime and covering energy span up to a GeV range of neutrino energies [42–44].

Whereas for the charged-current neutrino-nucleus reactions some experimental data are available for ^{12}C and ^{56}Fe [45–48], in the case of neutral-current inelastic neutrino-nucleus scattering there are no experimental data available, except for the ground state transition to the 15.11 MeV state ($T = 1$) in ^{12}C [49,50]. The indirect experimental insight into the inelastic neutrino-nucleus cross sections can be obtained from inelastic electron scattering. As shown in Ref. [51], magnetic dipole strength distributions for several iron group nuclei are dominated by isovector Gamow-Teller transitions that can be translated into inelastic neutral-current neutrino-nucleus cross sections. Due to a lack of direct experimental data on these cross sections, modeling by various approaches is crucial. In this way one can provide not only the relevant input for supernova simulations, but also the insight into theoretical uncertainties in a description of the cross sections in the neutral channel.

In this paper we introduce the framework for the neutral-current neutrino-nucleus inelastic scattering based on the relativistic nuclear energy density functional. Within this framework the nuclear ground state and various excitations induced in nuclei by the incoming neutrinos are described in a fully self-consistent approach, i.e., a universal effective interaction is employed without introducing any adjustments to the specific properties of target nuclei or neutrino energies involved. Although the energy density functional has already been employed in the nonrelativistic framework using Skyrme

parametrizations [31,32], the present study provides the first self-consistent framework to describe neutrino-induced reactions in the neutral channel, involving open-shell target nuclei that necessitate explicit implementation of the pairing correlations. The relativistic nuclear energy density functional has been successfully employed in studies of giant resonances and exotic modes of excitation [52–54], β-decay rates of r-process nuclei [55], muon capture [56] and stellar electron capture rates [11], and in constraining the neutron skin in nuclei [57]. In Refs. [9,58] the relativistic proton-neutron QRPA has been employed in modeling charged-current neutrino-nucleus reactions. In the present analysis of neutrino-induced reactions in the neutral channel, the model necessitates further development of the relativistic QRPA outlined in Ref. [59] in order to allow taking into account both natural and unnatural parity excitations in the neutral channel.

The paper is organized as follows. In Sec. II we introduce the basic formalism for the neutrino-nucleus cross sections in the neutral channel based on weak Hamiltonian and relativistic nuclear energy density functional. The respective cross sections have been explored in detail for a set of target nuclei in Sec. III. The conclusions of the present work are summarized in Sec. IV.

II. THEORETICAL BACKGROUND

The weak process to be considered is inelastic neutral-current neutrino-nucleus reaction,

$$\nu_e + {}_Z X_N \rightarrow \nu_e + {}_Z X_N^*, \tag{1}$$

where the incoming electron neutrino (ν_e) scatters on target nucleus $X(Z, N)$ which absorbs part of the neutrino energy. The interaction between the neutrino and nucleus is described by a weak Hamiltonian, while the properties of initial and final states of target nucleus are described by an effective nuclear interaction, in this particular case formulated using a relativistic energy density functional. The formalism leading to the expression for the cross section is given in Refs. [60,61]. The general expression for the neutrino-nucleus differential cross section is derived in terms of relevant multipoles of the nuclear weak currents,

$$\left(\frac{d\sigma_\nu}{d\Omega}\right) = \frac{G_F^2 \epsilon^2}{2\pi^2} \frac{4\pi}{2J_i + 1} \left\{ \sum_{J \geqslant 0} \{(1 - \hat{\boldsymbol{\nu}} \cdot \boldsymbol{\beta}) + 2(\hat{\boldsymbol{\nu}} \cdot \hat{\boldsymbol{q}})(\boldsymbol{\beta} \cdot \hat{\boldsymbol{q}})\langle J_f||\hat{\mathcal{L}}_J||J_i\rangle|^2 + (1 + \hat{\boldsymbol{\nu}} \cdot \boldsymbol{\beta})\langle J_f||\hat{\mathcal{M}}_J||J_i\rangle|^2 \right.$$
$$- 2\hat{\boldsymbol{q}}(\hat{\boldsymbol{\nu}} + \boldsymbol{\beta})\text{Re}\langle J_f||\hat{\mathcal{L}}_J||J_i\rangle\langle J_f||\hat{\mathcal{M}}_J||J_i\rangle^*\} + \sum_{J \geqslant 1} \{(1 - (\hat{\boldsymbol{\nu}} \cdot \hat{\boldsymbol{q}})(\boldsymbol{\beta} \cdot \hat{\boldsymbol{q}}))[|\langle J_f||\hat{\mathcal{T}}_J^{\text{MAG}}||J_i\rangle|^2 + |\langle J_f||\hat{\mathcal{T}}_J^{\text{EL}}||J_i\rangle|^2]$$
$$\left. + 2\hat{\boldsymbol{q}} \cdot (\hat{\boldsymbol{\nu}} - \boldsymbol{\beta})\text{Re}\langle J_f||\hat{\mathcal{T}}_J^{\text{MAG}}||J_i\rangle\langle J_f||\hat{\mathcal{T}}_J^{\text{EL}}||J_i\rangle^*\} \right\}, \tag{2}$$

where G_F is Fermi constant for the weak interaction and ϵ denotes the energy of outgoing neutrino. The momentum transfer $\boldsymbol{q} = \boldsymbol{\nu} - \boldsymbol{k}$ is defined as the difference between the incoming ($\boldsymbol{\nu}$) and outgoing ($\boldsymbol{k}$) neutrino momenta, $\hat{\boldsymbol{q}}$ and $\hat{\boldsymbol{\nu}}$ denote the corresponding unit vectors, and $\boldsymbol{\beta} = \boldsymbol{k}/\epsilon$. The transition matrix elements between the nuclear initial and final states include transition operators of various multipoles: charge $\hat{\mathcal{M}}_J$, longitudinal $\hat{\mathcal{L}}_J$, transverse electric $\hat{\mathcal{T}}_J^{\text{EL}}$, and

transverse magnetic $\hat{T}_J^{\mathrm{MAG}}$ multipole operators, expressed in terms of spherical Bessel functions, spherical harmonics, and vector spherical harmonics [60,61]. A complete calculation of inelastic neutrino-nucleus scattering necessitates the inclusion of a number of multipoles J. Although higher-order multipoles have rather small contributions at low incoming neutrino energies, these cannot be neglected at energies about tens of MeV [31,32,40]. In the present study, multipoles up to $J = 5$ contributing to the cross section in Eq. (2) will be included in calculations. In the specific case of the neutrino-nucleus scattering in the neutral channel, the transition operators listed above include the following form factors [33,62]:

(i) Vector form factors F_1^V, $\mu^V = F_1^V - 2MF_2^V$,

$$F_1^{V(n)}(q^2) = -\frac{1}{2}\left(1 + \frac{q^2}{(840 \text{ MeV})^2}\right)^{-2}, \qquad (3)$$

$$F_1^{V(p)}(q^2) = \frac{1}{2}(1 - 4\sin^2\theta_W)\left(1 + \frac{q^2}{(840 \text{ MeV})^2}\right)^{-2}, \quad (4)$$

$$\mu^{V(n,p)}(q^2) = \mu^{V(n,p)}(0)\left(1 + \frac{q^2}{(840 \text{ MeV})^2}\right)^{-2}. \qquad (5)$$

(ii) Axial vector form factor

$$F_A^{(n,p)}(q^2) = \mp\frac{1}{2}F_A(0)\left(1 + \frac{q^2}{(1032 \text{ MeV})^2}\right)^{-2}. \qquad (6)$$

(iii) Pseudoscalar form factor

$$F_P^{(n,p)}(q^2) = \frac{2m_N F_A^{(n,p)}(q^2)}{q^2 + m_\pi^2}. \qquad (7)$$

The indices n, p denote the respective form factors for neutrons and protons, θ_W denotes the Weinberg angle, $\sin^2\theta_W = 0.2325$, and the static values are $F_A(0) = -1.2617$, $\mu^{V(n)}(0) = -1.463$, and $\mu^{V(p)}(0) = 1.054$. In the present analysis the strange quark content in the form factors has been neglected. By employing the full operator structures in the transition matrix elements, the inelastic neutrino-nucleus cross section is evaluated using Eq. (2), with an additional quenching factor included in the free-nucleon axial-vector coupling constant, resulting in $F_A(0) = 1.0$. This quenching corresponds to additional factor 0.8 in F_A [Eq. (6)]. The value of the quenching depends on the effective interactions and the model space under consideration, e.g., in the hybrid model a quenching factor of 0.74 has been used [7], while 0.8 represents a reasonable value for the framework employed in the present study [9]. In a recent study [9], the shell model and nonrelativistic and relativistic (Q)RPA, prior to the implementation to neutrino-induced reactions, have been tested in modeling the GT$^+$ and GT$^-$ transition strengths. It has been shown that both in the GT$^+$ and GT$^-$ channels the quenching factor 0.8 in the axial vector coupling constant is necessary to reach the experimentally measured GT strengths (and the results from the shell model calculations which include the quenching factor 0.74). Therefore we employ $F_A(0) = 1.0$ in neutrino-nucleus interaction studies in this work.

The transition matrix elements between the initial and final states in Eq. (2) are determined in a fully self-consistent

framework based on a relativistic nuclear energy density functional [63,64]. Therein the nuclear ground state is described with the relativistic Hartree-Bogoliubov (RHB) model, and excited states are calculated using the relativistic quasiparticle random phase approximation (RQRPA) [53,59]. The application of relativistic nuclear energy density functional is realized in terms of the self-consistent mean field theory for nucleons and a minimal set of meson fields; isoscalar-scalar σ meson ($J^\pi = 0^+$, $T = 0$), isoscalar-vector ω meson ($J^\pi = 1^-$, $T = 0$), and the isovector-vector ρ meson ($J^\pi = 1^-$, $T = 1$), supplemented with the electromagnetic field. The meson-nucleon interaction is included with a minimal set of the interaction terms, where the vertex functionals include an explicit dependence on the vector density. The details of the RHB model based on this class of effective density-dependent interactions are given in Ref. [65]. For the model parameters that determine the density-dependent coupling strength and the meson masses we employ the values of the DD-ME2 parametrization, obtained by simultaneous adjustment of the effective interaction to the binding energies, charge radii, differences between radii of neutron and proton density distributions for 12 spherical nuclei, and nuclear matter properties at saturation density [66]. The pairing correlations in open shell nuclei are described by the finite range Gogny interaction, with parametrization D1S [67].

The RQRPA is formulated in the canonical single-nucleon basis of the RHB model, and the residual interaction is derived from the same nuclear energy density functional as in the RHB model [59,68]. In applications to finite nuclei, the relativistic models are used in the no-sea approximation, i.e., the Dirac sea of states with negative energies does not contribute to the densities and currents. In principle, one should also take into account the negative energy states, i.e., allow for a polarization of the vacuum. This leads to divergent terms, which have to be removed by a proper renormalization. In the case of finite nuclei, a local density approximation has been introduced [69], and semiclassical extensions of this method have been been used [70,71]. Recent approaches to the Dirac sea include, e.g., the implementation of the imaginary time step method [72] and construction of a no-sea effective theory from the underlying quantum field theory [73]. One should note that if one takes into account vacuum polarization, the parameter set of the Lagrangian has to be readjusted, and with new force one finds approximately the same results as in the case of neglecting vacuum polarization. This means that by fitting the parameters of the Lagrangian in the no-sea approximation a large part of the effect of the vacuum polarization is already taken into account. Most of the previous applications of the relativistic mean field theory to finite nuclei are done in the no-sea approximation [64], and the same approach is employed in this work. Accordingly, the RQRPA includes not only configurations composed from two-quasiparticle states of positive energy, but also pair-configurations formed from the fully or partially occupied states of positive energy and empty negative-energy states from the Dirac sea. In the implementation in modeling the weak interaction processes, the major advantage of the RHB + RQRPA model is that it is fully consistent in view of the effective interactions employed. In the particle-hole (ph) and pairing (pp) channels, the same

interactions are used in the RHB equations that determine the canonical quasiparticle basis, and in the matrix equations of the RQRPA. In this way, one can employ the same nuclear energy density functional in a description of the weak processes throughout the nuclide map without any additional adjustments of the model parameters.

In the present study we further extend the RQRPA framework outlined in Ref. [59] by including the pion contributions in order to account both for the natural, $(-1)^J = \pi$, and unnatural, $(-1)^{J+1} = \pi$, parity excitations that take part in inelastic neutrino-nucleus scattering. As shown in Refs. [38,40], unnatural parity excitations play an important role in the overall neutrino-nucleus cross sections in the neutral channel, and should be included in a framework aiming to provide consistent and reliable results. Excitations of unnatural parity states necessitate the inclusion of the residual interaction term generated by the π meson ($J^\pi = 0^-$, $T = 1$) exchange. At the Hartree level, i.e., in the RHB, the pion does not contribute because it carries unnatural parity and the corresponding mean field breaks parity. The pion major effect comes from the second- and higher-order diagrams in the correlated two-pion exchange. The quantum hadrodynamics model (QHD II) included, in addition to (σ, ω, ρ) meson fields, a pseudoscalar pion field as well. However, as pointed out in the RRPA study in Ref. [74], the pseudoscalar pion couples too strongly, resulting in total disruption of the ordering of the lowest excited states. The RRPA analysis showed that the implementation of pseudovector pion-nucleon coupling improves the spectrum in comparison to experiment, especially for the pion-like states $J^\pi = 0^-, 2^-, 4^-$.

Although the QHD has originally been introduced as a renormalizable quantum field theory, for the purpose of practical applications it is formulated as an effective, non-renormalizable quantum field theory representing the low-energy limit of the fundamental theory of strong interactions, namely, quantum chromodynamics (QCD) [75]. In order to allow a pseudovector pion-nucleon coupling, we drop the requirement of renormalizability. As pointed out in Ref. [76], a system of hadrons may in practice be better described by non-renormalizable or nonlocal field theory than a local renormalizable one. The pion-nucleon interaction with pseudovector coupling is given in the Lagrangian density as

$$\mathcal{L}_\pi^{(pv)} = \frac{f_\pi}{m_\pi} \bar\psi \gamma_5 \gamma^\mu \partial_\mu \vec\pi \vec\tau \psi \qquad (8)$$

and the propagator for the residual two-body interaction reads

$$D_\pi^{(pv)}(q) = -\frac{1}{q^2 + m_\pi^2}. \qquad (9)$$

The standard value for the pseudovector pion-nucleon coupling is $f_\pi^2/4\pi = 0.08$, while the measured pion mass amounts $m_\pi = 138$ MeV. Since the one-boson-exchange interaction with pseudovector coupling (8) contains a contact term, one accounts an additional term for the δ force to remove its contribution [53]. The two-body matrix elements of the one-pion exchange interaction and the δ force in pseudovector coupling are calculated in the momentum space representation according to a detailed formalism given in Ref. [77]. When calculating the neutrino-nucleus cross sections in Eq. (2),

for each transition operator $\hat O_J$ the matrix elements between the ground state and the final state of target nucleus are expressed in terms of single-particle matrix elements between quasiparticle canonical states, the corresponding occupation factors v_μ, u_μ and forward- and backward-going amplitudes X, Y, obtained by the diagonalization of the RQRPA matrix [59],

$$\langle J_f || \hat O_J || J_i \rangle = \sum_{\mu\mu'} \left\{ X_{\mu\mu'}^{J0} \langle \mu || \hat O_J || \mu' \rangle + (-1)^{j_\mu - j_{\mu'} + J} \right. $$
$$\left. \times Y_{\mu\mu'}^{J0} \langle \mu' || \hat O_J || \mu \rangle \right\} (u_\mu v_{\mu'} + (-1)^J v_\mu u_{\mu'}).$$
$$(10)$$

All relevant transitions between the $|0^+\rangle$ ground state and $|J_f^\pm\rangle$ final states are taken into account in the following calculations.

III. RESULTS AND DISCUSSION

We have employed the framework introduced in Sec. II in modeling the neutral-current neutrino-nucleus scattering for a set of target nuclei of interest for neutrino detector response and understanding the role of neutrinos in supernova evolution. In particular, the cross sections have been calculated as a function of the incoming neutrino energies for ^{12}C, ^{40}Ar, ^{56}Fe, ^{56}Ni, and $^{92-100}$Mo isotopes. The nuclear matrix elements are obtained using the energy density functional with DD-ME2 parametrization [66], supplemented by the Gogny force D1S to account for the pairing correlations in open shell nuclei [67]. The overall cross section Eq. (2) includes a summation over transitions to all possible final states characterized by multipoles up to $J = 5$ with both positive and negative parity.

In Fig. 1 the calculated electron neutrino-nucleus cross sections are showed for the inelastic scattering ^{12}C(ν_e, ν_e')^{12}C* for the range of neutrino energies $E_\nu = 0-100$ MeV. A
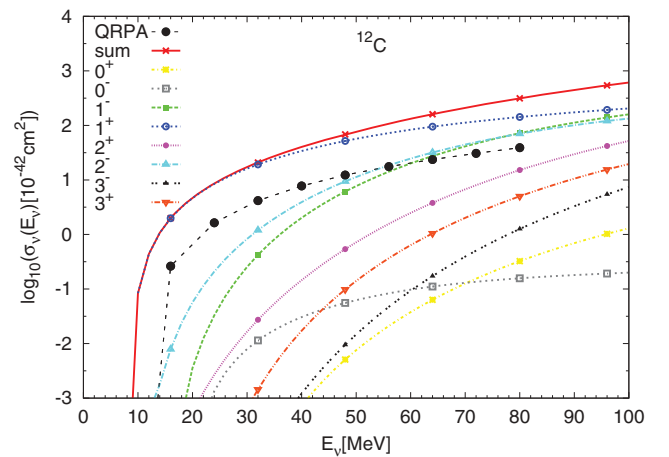
FIG. 1. (Color online) Dependence of the neutrino-nucleus cross sections for the scattering process ^{12}C(ν_e, ν_e')^{12}C* on the incoming neutrino energy. The cross sections with separate contributions from various multipoles $J_\pi = 0^\pm - 3^\pm$ and the total cross sections, including $J_\pi = 0^\pm - 5^\pm$ states, are shown. The overall cross sections (stars) are shown in comparison to the QRPA based results (full circles) from Ref. [38].
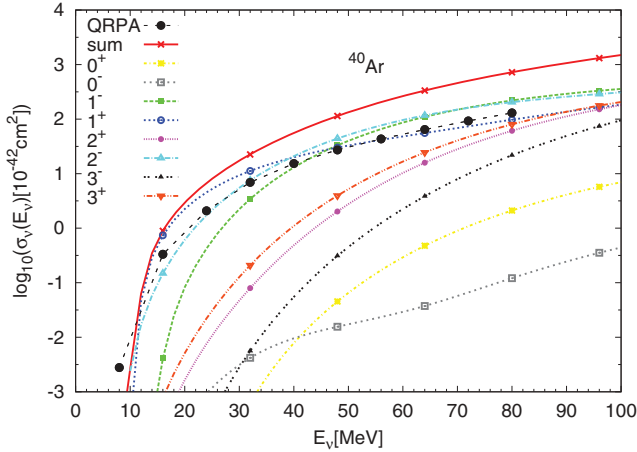
FIG. 2. (Color online) The same as in Fig. 1, but for the scattering process ^{40}Ar$(\nu_e, \nu_e')^{40}$Ar*. The overall cross sections (stars) are shown in comparison to the QRPA based results (full circles) from Ref. [40].

FIG. 3. (Color online) The same as in Fig. 1, but for the scattering process ^{56}Fe$(\nu_e, \nu_e')^{56}$Fe*.

complete set of multipole states $J^\pi = 0^\pm$–$5^\pm$ is taken into account in the overall cross section. Various contributions from the most relevant multipole states $J^\pi = 0^\pm$–$3^\pm$ to the cross sections are also displayed separately. For comparison, Fig. 1 also shows recent results for the overall cross sections for ^{12}C target, based on a QRPA with Bonn CD potential [38]. As one can observe in this figure, at low neutrino energies the overall cross sections are dominated by 1^+ transitions. However, as the energy increases to 100 MeV, the role of other multipoles becomes important, in particular those of 1^-, 2^-, and smaller contributions from 2^+ states. In the specific case of neutrino energy $E_\nu = 50$ MeV, the present results are at variance with Ref. [31], where the multipole contribution from $J^\pi = 1^-$ dominates over 1^+. On the other hand, the multipole composition of the cross sections is in qualitative agreement with a recent study based on the QRPA [38]. The total cross sections from the present study appear systematically larger than the respective values obtained using the QRPA [38]. We turn to this discrepancy later in a discussion of the cross sections.

In Fig. 2 the cross sections are shown for the scattering process ^{40}Ar$(\nu_e, \nu_e')^{40}$Ar*. In comparison to ^{12}C, the interplay between various multipoles becomes more involved. Although at low energies 1^+ transitions dominate, at E_ν above $\approx$ 40 MeV, 1^- and 2^- multipoles have the largest contributions. Neutrino-induced reactions with ^{40}Ar have been studied in detail in a recent work based on QRPA [40], in view of their relevance for detecting core-collapsing supernovae neutrinos. For comparison, the respective QRPA results from Ref. [40] are also shown in Fig. 2. The total cross sections from the present analysis appear up to an order of magnitude larger than the QRPA [40] ones. Even though a variety of advanced theoretical frameworks have been developed over the past years, one can observe considerable theoretical uncertainty inherent in the modeling of the neutral-current neutrino-nucleus cross sections. These uncertainties originate to a large extent to differences in single-particle spectra and respective transitions induced by incoming neutrinos. In Ref. [32] it has been shown that even within the same model, Hartree-Fock +
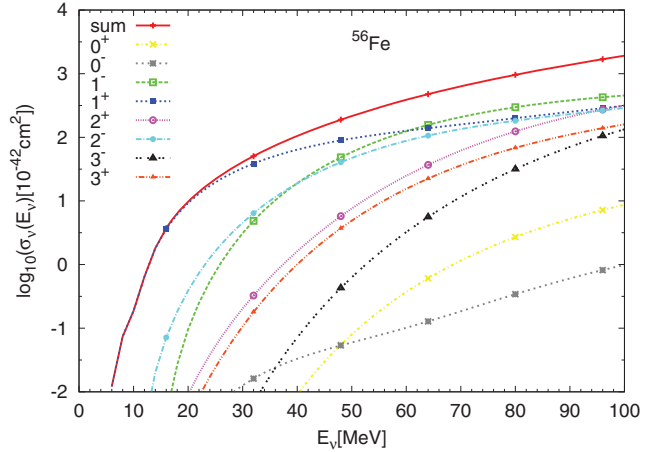
RPA based on Skyrme functional, only a small adjustment of single-particle parameters resulted in a 30% increase of the overall neutral-current neutrino-nucleus cross sections. Therefore, it is not surprising that an implementation of various models using independent effective interactions could result in large differences. Consequently, it is important to provide a reasonable quantitative estimate of theoretical uncertainty in the cross sections and to critically assess its effect in modeling supernova evolution and neutrino detector response. In a recent analysis of charged-current neutrino-nucleus cross sections [9], by employing a variety of microscopic models and effective interactions, it has been shown that one can provide a reasonable estimate of the theoretical uncertainty in modeling weak interaction processes.

Figures 3 and 4 show the neutral-current neutrino-^{56}Fe and -^{56}Ni cross sections, respectively. Although the multipole composition of the cross sections appear in qualitative agreement, some smaller differences can be noted due to differences in neutron and proton numbers and respective excitation spectra. However, one can conclude as a general property that $J = 1$ states are the most dominant, at lower energies $J^\pi = 1^+$
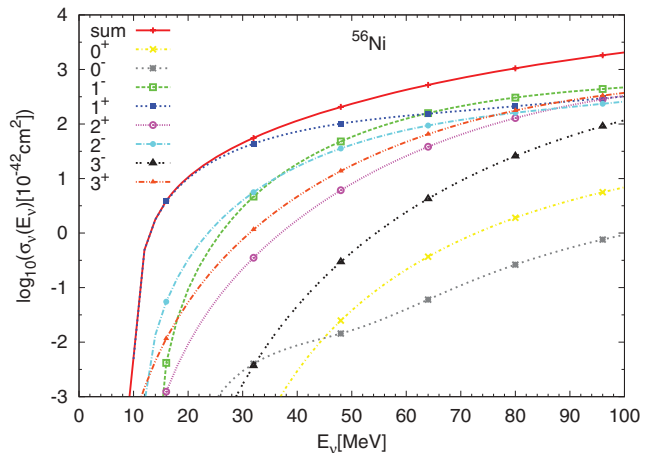

FIG. 4. (Color online) The same as in Fig. 1, but for the scattering process ^{56}Ni$(\nu_e, \nu_e')^{56}$Ni*.

TABLE I. The cross sections for the ^{56}Fe$(\nu_e, \nu'_e)^{56}$Fe* process, given in units of 10^{-42} cm^2. The results of the present analysis without (second column) and with the quenching factor (0.8) in F_A (third column) are compared with the results of the hybrid model [30] (fourth column) and QRPA based model from Ref. [34] (fifth column).

E_ν [MeV]	w/o quench.	w quench.	Hybrid [30]	QRPA [34]
10	2.91(-1)	1.87(-1)	1.91(-1)	1.01($+0$)
20	1.51($+1$)	9.78($+0$)	6.90($+0$)	5.79($+0$)
30	6.26($+1$)	4.08($+1$)	2.85($+1$)	1.87($+1$)
40	1.57($+2$)	1.05($+2$)	7.86($+1$)	5.51($+1$)
50	3.24($+2$)	2.16($+2$)	1.72($+2$)	1.43($+2$)
60	5.76($+2$)	3.89($+2$)	3.20($+2$)	3.09($+2$)
70	9.29($+2$)	6.33($+2$)	5.25($+2$)	5.63($+2$)
80	1.40($+3$)	9.59($+2$)	7.89($+2$)	8.82($+2$)
90	2.00($+3$)	1.38($+3$)	1.11($+3$)	1.22($+3$)
100	2.76($+3$)	1.92($+3$)	1.49($+3$)	1.52($+3$)

dominates while at $E_\nu \gtrsim 65$ MeV transitions $J^\pi = 1^-$ have the major contribution. In addition, at higher energies the $J^\pi = 2^-$ state also competes with $J^\pi = 1^-$ for dominance. At high-end neutrino energy ≈ 100 MeV other multipole transitions also contribute to the overall cross sections, e.g., $J^\pi = 2^\pm, 3^\pm$. The calculated cross sections for the scattering process ^{56}Fe$(\nu_e, \nu'_e)^{56}$Fe* are explored in detail in comparison with the hybrid model [30] and QRPA based framework [34]. In Table I the RQRPA cross sections are given for a selection of neutrino energies up to 100 MeV. For comparison, the results are shown both with and without quenching in F_A [Eq. (6)]. It is interesting to observe that at low neutrino energies, where the cross sections are rather sensitive on the fine details of the transition spectra, the RQRPA (with quenching) and hybrid model results are in excellent agreement. Although the cross sections from the three models appear in the overall qualitative agreement, in the energy region of relevance for the supernova neutrino processes (≈ 20–40 MeV) the RQRPA cross sections are up to a factor ≈ 1.5 (2.0) larger than the hybrid model and QRPA results, respectively. It is interesting to note that a very recent QRPA study resulted in averaged cross sections for ^{56}Fe roughly a factor of two larger than for the hybrid model [37].

The scattering cross sections in the neutral channel have also been explored for a set of Mo isotopes, that recently became interesting due to ongoing and future applications of molybdenum in terrestrial neutrino detectors, MOON [12] and NEMO [14], related to neutrino studies and search for the events of neutrinoless double β decay. In the present analysis the cross sections have been explored for the most abundant even molybdenum isotopes, ^{92}Mo, ^{94}Mo, ^{96}Mo, ^{98}Mo, and ^{100}Mo. The major contribution in natural molybdenum comes from ^{98}Mo, amounting 24.13%. Table II shows the neutral-current neutrino-nucleus cross sections for even isotopes $^{92-100}$Mo in the range of incoming neutrino energy $E_{\nu_e} =$ 10–100 MeV. By inspecting the numbers, one can observe a rather small but systematic increase in the cross section values for all neutrino energies. As can be expected, ^{100}Mo has the largest cross section of all shown so far simply by virtue of a large number of active nucleons contributing to the collective nuclear response in the scattering process. The respective

TABLE II. The total neutral-current neutrino-nucleus cross sections for even isotopes $^{92-100}$Mo, given in units of 10^{-42} cm^2.

E_ν [MeV]	^{92}Mo	^{94}Mo	^{96}Mo	^{98}Mo	^{100}Mo
10	6.32(-2)	3.58(-1)	5.25(-1)	6.67(-1)	7.82(-1)
20	9.68($+0$)	1.14($+1$)	1.21($+1$)	1.26($+1$)	1.29($+1$)
30	4.98($+1$)	5.42($+1$)	5.59($+1$)	5.73($+1$)	5.84($+1$)
40	1.46($+2$)	1.55($+2$)	1.59($+2$)	1.63($+2$)	1.67($+2$)
50	3.22($+2$)	3.39($+2$)	3.47($+2$)	3.56($+2$)	3.64($+2$)
60	5.89($+2$)	6.16($+2$)	6.32($+2$)	6.47($+2$)	6.61($+2$)
70	9.49($+2$)	9.88($+2$)	1.01($+3$)	1.03($+3$)	1.06($+3$)
80	1.40($+3$)	1.45($+3$)	1.48($+3$)	1.51($+3$)	1.54($+3$)
90	1.92($+3$)	1.99($+3$)	2.03($+3$)	2.07($+3$)	2.11($+3$)
100	2.52($+3$)	2.61($+3$)	2.66($+3$)	2.71($+3$)	2.75($+3$)

cross sections for ^{98}Mo and their multipole compositions are displayed in Fig. 5. For neutrino energies below 10 MeV both 0^- and 1^+ states have relevant contributions. At $E_\nu \approx$ 45 MeV one can observe the intersection between the main components in the cross sections: 1^+ at lower energies and 1^-, 2^- which dominate at higher energies. When comparing the overall cross sections to those of other recent studies based on QRPA [37,40], the present results are systematically larger, but within an order of magnitude.

In order to explore theoretical uncertainties in modeling neutral-current neutrino-nucleus reactions in more detail, in Figs. 6 and 7 partial multipole contributions to the cross sections for ^{96}Mo target are shown at incoming electron neutrino energies $E_{\nu_e} = 20$ and 100 MeV, respectively. The results of the present study (RQRPA) are shown in comparison with the cross sections recently obtained using QRPA (Balasi *et al.*, Ref. [37]). Although the total RQRPA cross sections are somewhat larger than those of QRPA, one can observe to a large extent excellent qualitative agreement between the two models based on rather different backgrounds. At low neutrino energy (Fig. 6) in both cases a largely dominant excitation channel is 1^+. The distribution over various multipoles appears rather involved at $E_{\nu_e} = 100$ MeV. The main contribution is obtained for 1^- transitions, but other multipoles also show
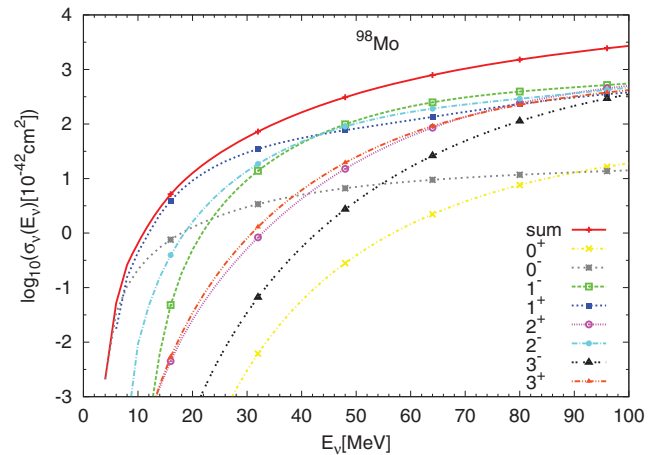

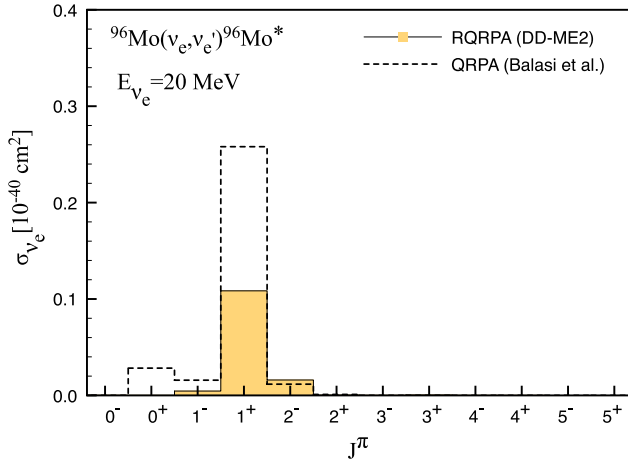FIG. 5. (Color online) The same as in Fig. 1, but for the scattering process ^{98}Mo$(\nu_e, \nu'_e)^{98}$Mo*.

FIG. 6. (Color online) Contributions of multipole transitions $J^{\pi} = 0^{\pm}$–$5^{\pm}$ in the cross sections for the reaction ^{96}Mo$(\nu_e, \nu_e')^{96}$Mo* at incoming electron neutrino energy $E_{\nu_e} = 20$ MeV. The results of the present analysis (RQRPA) are compared with QRPA based calculations (Balasi *et al.*, Ref. [37]).

considerable effects, ranked in the order of importance as follows: 1^-, 2^+, 2^-, 1^+, 3^+, 3^-, etc. The models based on RQRPA and QRPA result in excellent agreement in relative contributions of various multipoles, except for the anomaly for the QRPA 1^+ channel.

An important application of microscopic models of neutrino-nucleus reactions is a description of the cross sections for stellar neutrinos of relevance for the neutrino detectors that could provide better insight into fascinating events in the universe that produce neutrinos. The calculated cross sections given as functions of the incoming neutrino energy can be averaged over supernova neutrino flux, that is usually described by the Fermi-Dirac distribution,

$$f(E_\nu) = \frac{1}{T^3}\frac{E_\nu^2}{\exp[(E_\nu/T) - \alpha] + 1}\ . \qquad (11)$$

Especially interesting is modeling the reaction rates of neutrinos scattering on nuclei that can be used as targets
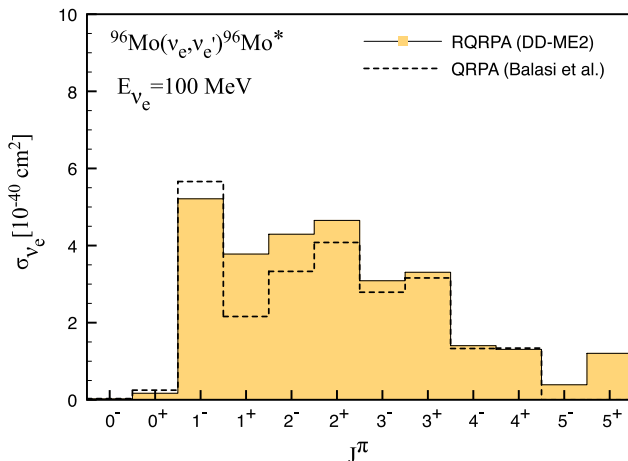

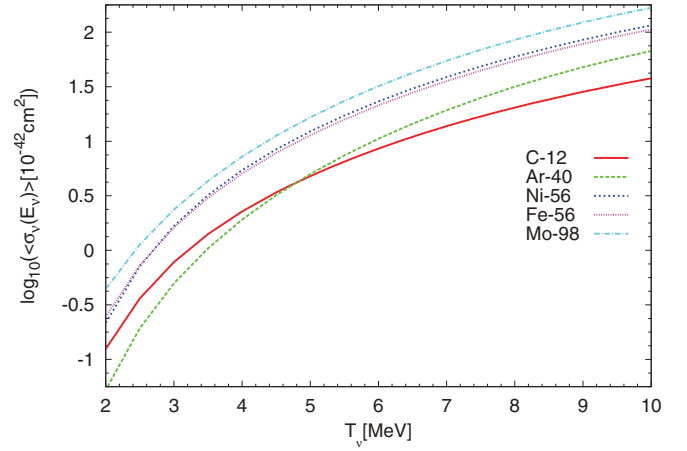FIG. 7. (Color online) The same as in Fig. 6, but for the neutrino energy $E_{\nu_e} = 100$ MeV.

FIG. 8. (Color online) Neutral-current neutrino-nucleus cross sections averaged over the supernova neutrino flux in the temperature interval $T_\nu = 2$–10 MeV. Results are shown for ^{12}C, ^{40}Ar, ^{56}Fe, ^{56}Ni, and ^{98}Mo target nuclei.

for the supernova neutrino detectors, e.g., ^{40}Ar, ^{56}Fe, ^{56}Ni, Mo isotopes, etc. In this way, one can predict an expected number of events in the detector that originate from a specific stellar environment which determines the production of low-energy neutrinos. In this work we calculate the neutral-current neutrino-nucleus cross sections averaged over the supernova neutrino flux in the range of temperatures $T_\nu = 2$–10 MeV, and for the chemical potential $\alpha = 0$. Figure 8 shows the respective flux-averaged cross sections for a set of target nuclei, ^{12}C, ^{40}Ar, ^{56}Fe, ^{56}Ni, and ^{98}Mo. As the temperature increases, neutrinos with higher energies have larger contributions in the averaged cross sections. The reason is twofold: (i) the Fermi-Dirac distribution shifts toward higher energies with increased temperature, and (ii) the neutrino-nucleus cross sections increase with neutrino energy and contributions of higher multipole transitions become significant. In general, for heavier target nuclei the overall cross sections are more pronounced. In view of the modern neutrino detectors based on molybdenum, it is interesting to inspect the results of mi-
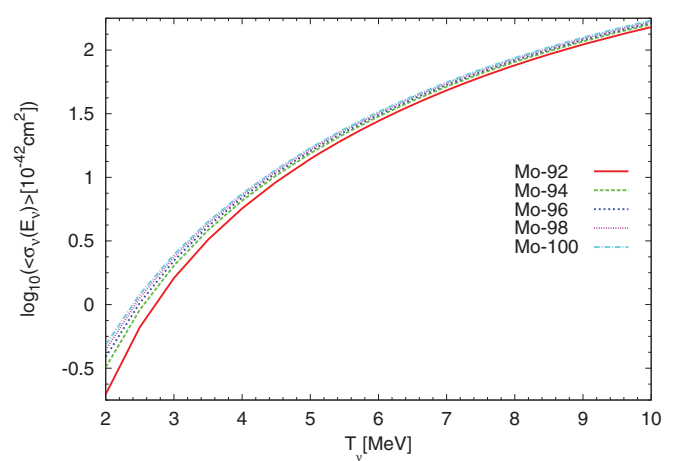

FIG. 9. (Color online) The same as in Fig. 8 but for ^{92,94,96,98,100}Mo target nuclei.

croscopic calculations for the processes induced by supernova neutrinos in the most abundant Mo isotopes. In Fig. 9 the respective cross sections, obtained by folding with the Fermi-Dirac distribution (11) for $\alpha = 0$, are shown as a function of temperature for even isotopes $^{92-100}$Mo. In accordance with the cross sections shown in Table II, the averaged cross sections increase with the number of neutrons in the Mo isotope chain. However, the differences between the averaged cross sections are more pronounced at lower temperatures due to a larger sensitivity of the cross sections to the transitions involved. For example, the ratio $\langle\sigma(^{100}\text{Mo})\rangle/\langle\sigma(^{92}\text{Mo})\rangle =$ (2.46, 1.31, 1.18, 1.14, 1.13) for the set of temperatures $T =$ (2, 4, 6, 8, 10) MeV, respectively.

IV. CONCLUSION

In summary, modeling of the neutrino-nucleus scattering through the weak neutral current provides important data for simulations of supernova evolution and detector response to neutrinos emerging from explosive stellar events. Due to a lack of experimental data, it is necessary to provide independent microscopic insights into the properties of neutrino-induced processes, and assess the theoretical uncertainty inherent to the implementation of various nuclear effective interactions which determine the transition matrix elements contributing to the neutrino-nucleus cross sections in the neutral channel.

In this work the self-consistent framework for inelastic neutral-current neutrino-nucleus scattering is introduced, based on a systematic implementation of the relativistic nuclear energy density functional with density dependent meson-nucleon couplings. The cross sections have been formulated using the weak interaction Hamiltonian and nuclear properties of initial and excited states are obtained by using the RHB + RQRPA, thus allowing studies of open shell target nuclei that necessitate the explicit inclusion of the pairing correlations. In order to include a complete set of natural and unnatural parity excited states, the RQRPA residual interaction has been extended using the pion contributions with pseudovector coupling. In the present analysis, the neutral-current neutrino-nucleus cross sections have been calculated for the set of target nuclei, ^{12}C, ^{40}Ar, ^{56}Fe, and ^{56}Ni. In addition, in view of the MOON [12] and NEMO [14] experiments based on molybdenum detectors, the present study covered the respective neutrino-nucleus cross sections in the neutral

channel for the most abundant even isotopes $^{92-100}$Mo. In addition to Tables I and II presented in this work, complete tables of all calculated cross sections with a small step in neutrino energy are available on request.

A comparison of the cross sections and their multipole composition appear to be in reasonable agreement with previous studies, however, some quantitative differences have been observed. From the comparison with calculations based on the hybrid model and QRPA, the present analysis provides an estimate of the theoretical uncertainty in modeling the cross sections in the neutral channel due to the implementation of various theoretical frameworks and nuclear effective interactions. In the case of ^{56}Fe, it is shown that the overall cross sections exhibit variations, i.e., at some neutrino energies the cross sections based on RQRPA, QRPA, and the hybrid model can differ by a factor ≈ 2. This result, together with discrepancies up to an order of magnitude between the RQRPA and QRPA calculations shown for ^{12}C and ^{40}Ar, indicates that in future studies one could critically assess the effect of uncertainties emerging from the calculated cross sections on supernova evolution models or neutrino detector response.

The main advantage of the present approach to the neutrino-nucleus cross sections in the neutral channel is the self-consistent modeling of all relevant transition matrix elements involving open-shell nuclei, without any additional adjustments of the model parameters to the nuclear target under consideration. In this way, the present study paves the way for systematic self-consistent large-scale calculations of stellar neutrino-nucleus scattering in the neutral channel. However, this goal would also necessitate a further extension of the model, in order to include the finite temperature effects in a description of nuclei and their excited states in the supernova environment. As shown in Refs. [7,23], at finite temperature the cross sections become somewhat enhanced at lower neutrino energies. In the forthcoming study, the present theoretical framework will be extended to include finite temperature effects, typical for the supernova environment.

[1] H.-Th. Janka, K. Langanke, A. Marek, G. Martinez-Pinedo, and B. Müller, Phys. Rep. **442**, 38 (2007).

[2] S. E. Woosley, D. H. Hartmann, R. D. Hoffman, and W. C. Haxton, Astrophys. J. **356**, 272 (1990).

[3] W. C. Haxton, Phys. Rev. Lett. **60**, 1999 (1988).

[4] S. W. Bruenn and W. C. Haxton, Astrophys. J. **376**, 678 (1991).

[5] K. Langanke, G. Martinez-Pinedo, B. Müller, H.-Th. Janka, A. Marek, W. R. Hix, A. Juodagalvis, and J. M. Sampaio, Phys. Rev. Lett. **100**, 011101 (2008).

[6] K. Langanke, Nucl. Phys. A **834**, 608c (2010).

[7] A. Juodagalvis, K. Langanke, G. Martinez-Pinedo, W. R. Hix, D. J. Dean, and J. M. Sampaio, Nucl. Phys. A **747**, 87 (2005).

[8] A. R. Samana, F. Krmpotić, N. Paar, and C. A. Bertulani, Phys. Rev. C **83**, 024303 (2011).

[9] N. Paar, T. Suzuki, M. Honma, T. Marketin, and D. Vretenar, Phys. Rev. C **84**, 047305 (2011).

[10] N. Paar, G. Colo, E. Khan, and D. Vretenar, Phys. Rev. C **80**, 055801 (2009).

[11] Y. F. Niu, N. Paar, D. Vretenar, and J. Meng, Phys. Rev. C **83**, 045807 (2011).

[12] H. Ejiri *et al.*, Eur. Phys. J. Special Topics **162**, 239 (2008).

[13] A. A. Aguilar-Arevalo *et al*. (MiniBooNE Collaboration), Nucl. Instrum. Methods Phys. Res. A **599**, 28 (2009).

[14] R. Arnold *et al*., Phys. Rev. Lett. **95**, 182302 (2005).

[15] P. Adamson *et al*., Phys. Rev. D **73**, 072002 (2006).

[16] C. Kraus (SNO+ Collaboration), Prog. Part. Nucl. Phys. **64**, 273 (2010).

[17] N. Agafonova *et al*., Phys. Lett. B **691**, 138 (2010).

[18] N. Yu Agafonova *et al*., Astron. Phys. **27**, 254 (2007).

[19] Y. Efremenko, Nucl. Phys. B, Proc. Suppl. **138**, 343 (2005); F. T. Avignone III and Y. V. Efremenko, J. Phys. G **29**, 2615 (2003).

[20] D. A. Harris (MINOS NOvA. Collaborations), Nucl. Phys. B, Proc. Suppl. **149**, 150 (2005).

[21] S. Ying, W. C. Haxton, and E. M. Henley, Phys. Rev. C **45**, 1982 (1992).

[22] J. Engel, E. Kolbe, K. Langanke, and P. Vogel, Phys. Rev. C **54**, 2740 (1996).

[23] J. M. Sampaio, K. Langanke, G. Martinez-Pinedo, and D. J. Dean, Phys. Lett. B **529**, 19 (2002).

[24] T. Yoshida, T. Suzuki, S. Chiba, T. Kajino, H. Yokomakura, K. Kimura, A. Takamura, and D. H. Hartmann, Astrophys. J. **686**, 448 (2008).

[25] T. Suzuki, M. Honma, K. Higashiyama, T. Yoshida, T. Kajino, T. Otsuka, H. Umeda, and K. Nomoto, Phys. Rev. C **79**, 061603(R) (2009).

[26] T. Suzuki, M. Honma, T. Yoshida, H. Mao, T. Kajino, and T. Otsuka, Prog. Part. Nucl. Phys. **66**, 385 (2011).

[27] A. Hektor, E. Kolbe, K. Langanke, and J. Toivanen, Phys. Rev. C **61**, 055803 (2000).

[28] K. Langanke and E. Kolbe, At. Data Nucl. Data Tables **82**, 191 (2002).

[29] J. Toivanen, E. Kolbe, K. Langanke, G. Martinez-Pinedo, and P. Vogel, Nucl. Phys. A **694**, 395 (2001).

[30] E. Kolbe, K. Langanke, G. Martinez-Pinedo, and P. Vogel, J. Phys. G **29**, 2569 (2003).

[31] N. Jachowicz, S. Rombouts, K. Heyde, and J. Ryckebusch, Phys. Rev. C **59**, 3246 (1999).

[32] N. Jachowicz, K. Heyde, and J. Ryckebusch, Phys. Rev. C **66**, 055501 (2002).

[33] V. C. Chasioti and T. S. Kosmas, Nucl. Phys. A **829**, 234 (2009).

[34] V. C. Chasioti, T. S. Kosmas, and P. C. Divari, Prog. Part. Nucl. Phys. **59**, 481 (2007).

[35] P. C. Divari, V. C. Chasioti, and T. S. Kosmas, Phys. Scr. **82**, 065201 (2010).

[36] V. Tsakstara and T. S. Kosmas, Phys. Rev. C **83**, 054612 (2011).

[37] K. G. Balasi, E. Ydrefors, and T. S. Kosmas, Nucl. Phys. A **868**, 82 (2011).

[38] Myung-Ki Cheoun, Eunja Ha, K. S. Kim, and Toshitaka Kajino, J. Phys. G **37**, 055101 (2010).

[39] Myung-Ki Cheoun, Eunja Ha, T. Hayakawa, T. Kajino, and S. Chiba, Phys. Rev. C **82**, 035504 (2010).

[40] Myung-Ki Cheoun, Eunja Ha, and Toshitaka Kajino, Phys. Rev. C **83**, 028801 (2011).

[41] M. S. Athar, S. Ahmad, and S. K. Singh, Phys. Rev. C **71**, 045501 (2005).

[42] A. N. Antonov, M. V. Ivanov, M. B. Barbaro, J. A. Caballero, E. Moya de Guerra, and M. K. Gaidarov, Phys. Rev. C **75**, 064617 (2007).

[43] J. E. Amaro, M. B. Barbaro, J. A. Caballero, and T. W. Donnelly, Phys. Rev. C **73**, 035503 (2006).

[44] Andrea Meucci, Carlotta Giusti, and Franco Davide Pacati, Phys. Rev. D **84**, 113003 (2011).

[45] C. Athanassopoulos *et al*., Phys. Rev. C **55**, 2078 (1997).

[46] B. E. Bodmann *et al*., Phys. Lett. B **332**, 251 (1994).

[47] R. Maschuw, Prog. Part. Nucl. Phys. **40**, 183 (1998).

[48] D. D. Koetke *et al*., Phys. Rev. C **46**, 2554 (1992).

[49] B. Zeitnitz, Prog. Part. Nucl. Phys. **32**, 351 (1994).

[50] L. B. Auerbach *et al*., Phys. Rev. C **64**, 065501 (2001).

[51] K. Langanke, G. Martinez-Pinedo, P. von Neumann-Cosel, and A. Richter, Phys. Rev. Lett. **93**, 202501 (2004).

[52] D. Vretenar, P. Ring, G. A. Lalazissis, and N. Paar, Nucl. Phys. A **649**, 29c (1999).

[53] N. Paar, D. Vretenar, E. Khan, and G. Colo, Rep. Prog. Phys. **70**, 691 (2007).

[54] E. Khan, N. Paar, and D. Vretenar, Phys. Rev. C **84**, 051301(R) (2011).

[55] T. Nikšić, T. Marketin, D. Vretenar, N. Paar, and P. Ring, Phys. Rev. C **71**, 014308 (2005).

[56] T. Marketin, N. Paar, T. Nikšić, and D. Vretenar, Phys. Rev. C **79**, 054323 (2009).

[57] A. Klimkiewicz *et al*., Phys. Rev. C **76**, 051603(R) (2007).

[58] N. Paar, D. Vretenar, T. Marketin, and P. Ring, Phys. Rev. C **77**, 024608 (2008).

[59] N. Paar, P. Ring, T. Nikšić, and D. Vretenar, Phys. Rev. C **67**, 034312 (2003).

[60] J. S. O'Connel, T. W. Donnelly, and J. D. Walecka, Phys. Rev. C **6**, 719 (1972).

[61] J. D. Walecka, in *Muon Physics*, edited by V. M. Hughes and C. S. Wu (Academic, New York, 1975).

[62] S. K. Singh, Nucl. Phys. B, Proc. Suppl. **112**, 77 (2002).

[63] T. Nikšić, D. Vretenar, and P. Ring, Phys. Rev. C **78**, 034318 (2008).

[64] D. Vretenar, A. Afanasjev, G. A. Lalazissis, and P. Ring, Phys. Rep. **409**, 101 (2005).

[65] T. Nikšić, D. Vretenar, P. Finelli, and P. Ring, Phys. Rev. C **66**, 024306 (2002).

[66] G. A. Lalazissis, T. Nikšić, D. Vretenar, and P. Ring, Phys. Rev. C **71**, 024312 (2005).

[67] J. Berger, M. Girod, and D. Gogny, Comput. Phys. Commun. **63**, 365 (1991).

[68] T. Nikšić, D. Vretenar, and P. Ring, Phys. Rev. C **66**, 064302 (2002).

[69] C. J. Horowitz and B. D. Serot, Phys. Lett. B **140**, 181 (1984).

[70] D. A. Wasson, Phys. Lett. B **210**, 41 (1988).

[71] Z. Y. Zhu, H. J. Mang, and P. Ring, Phys. Lett. B **254**, 325 (1991).

[72] Y. Zhang, H. Z. Liang, and J. Meng, Int. J. Mod. Phys. E **19**, 55 (2010).

[73] F. Karbstein, Phys. Rev. C **81**, 045206 (2010).

[74] R. J. Furnstahl, Phys. Lett. B **152**, 313 (1985).

[75] B. D. Serot and J. D. Walecka, Adv. Nucl. Phys. **16**, 1 (1986).

[76] J. I. Kapusta, Phys. Rev. C **23**, 1648 (1981).

[77] M. Serra, doctoral thesis, Universitätsbibliothek PHY 454d, Technische Universität München (2001).